

## Research Paper

# Reduced material model for closed cell metal foam infiltrated with phase change material based on high resolution numerical studies



Christoph Ohsenbrügge<sup>a,\*</sup>, Wieland Marth<sup>b</sup>, Iñaki Navarro y de Sosa<sup>a</sup>,  
Welf-Guntram Drossel<sup>a</sup>, Axel Voigt<sup>b</sup>

<sup>a</sup> Professorship for Adaptronics and Lightweight Design, TU Chemnitz, 09111 Chemnitz, Germany

<sup>b</sup> Institut für Wissenschaftliches Rechnen, TU Dresden, 01062 Dresden, Germany

## HIGHLIGHTS

- Closed cell metal foam sandwich structures were investigated.
- High resolution numerical studies were conducted using CT scan data.
- A reduced model for use in commercial FE software reduces needed degrees of freedom.
- Thermal inertia is increased about 4 to 5 times in PCM filled structures.
- The reduced material model was verified using experimental data.

## ARTICLE INFO

## Article history:

Received 17 December 2014

Accepted 28 September 2015

Available online 23 October 2015

## Keywords:

Metal foam

Phase change material

Diffuse domain approach

## ABSTRACT

The thermal behaviour of closed cell metal foam infiltrated with paraffin wax as latent heat storage for application in high precision tool machines was examined. Aluminium foam sandwiches with metallurgically bound cover layers were prepared in a powder metallurgical process and cross-sectional images of the structures were generated with X-ray computed tomography. Based on the image data a three dimensional highly detailed model was derived and prepared for simulation with the adaptive FE-library AMDiS. The pores were assumed to be filled with paraffin wax. The thermal conductivity and the transient thermal behaviour in the phase-change region were investigated. Based on the results from the highly detailed simulations a reduced model for use in commercial FE-software (ANSYS) was derived. It incorporates the properties of the matrix and the phase change material into a homogenized material. A sandwich-structure with and without paraffin was investigated experimentally under constant thermal load. The results were used to verify the reduced material model in ANSYS.

© 2015 Published by Elsevier Ltd.

## 1. Introduction

In high precision mechanical engineering thermal deformations have a large impact on machining accuracy. The fraction of geometrical errors attributed to thermal effects caused by inner and outer heat sources stayed constant in the last decades at about 70–75% [1,2]. While active cooling mechanisms are well established for temperature control to counteract these problems, they are responsible for a large share of energy consumption of the tool machine. In order to increase the energy-efficiency, standby-concepts which allow for a deactivation of basic loads such as the cooling system are a promising approach yet they have the disadvantage of putting the thermal stability and therefore the accuracy of the tool machine at risk [3]. Solutions that reduce the impact of thermal effects on

the accuracy without large demands for energy could solve this problem.

Phase change materials (PCM) offer the possibility to stabilize thermal behaviour by providing an increased thermal inertia in its melting range. The latent heat of the phase change enables the material to store or release large amounts of heat over a narrow temperature range [4]. The application of increased thermal inertia is being investigated and used in civil engineering to smooth the temperature variation in interior spaces, as cooling or heating element in transport and storage containers [5] and as heat sink for electronic components [6,7].

Due to the low thermal conductivity of most PCMs and especially paraffin based ones, a non-uniform heating inside a storage volume occurs with the melting interface moving away from the heat source. This leads to a limitation in terms of absorbable or releasable heat per time. Another typical problem with solid-liquid phase change is the mechanical stability of the material as well as the volume change during the melting process [7]. Paraffin-based

\* Corresponding author. Tel.: +49 35147722342.

E-mail address: [christoph.ohsenbruegge@mb.tu-chemnitz.de](mailto:christoph.ohsenbruegge@mb.tu-chemnitz.de) (C. Ohsenbrügge).

PCMs show a volume expansion in the order of 10%. A common approach to counteract these problems is encapsulation of the material or the usage of additives with high thermal conductivity. For an overview of published research on different approaches, see References 8 and 9. Notably Mills et al. [6] used expanded graphite as matrix material in a cooling concept for Li-Ion battery packs, metallic meshes were considered by Shuja et al. [10] and SiC ceramic honeycomb by Li et al. [11]. While open cell metal foams also received some attention [12,13], closed cell foams are also a viable, yet not well investigated option. Wang et al. [4] conducted experiments on paraffin/aluminium foam composites showing an improvement in melting time and temperature distribution in the composite PCM while they recommend the development of thermal models to simulate the heat storage process of the composite.

Closed cell metal foam is suitable as matrix material due to micro cracks in the walls of the individual pores, making infiltration of liquid paraffin based PCM into the pores of closed cell foam possible. The composite thermal storage exhibits a good mechanical stability while improving the thermal performance. Metal foams are a material class with low densities and novel mechanical, thermal, electrical and acoustical properties [14]. Furthermore a powder-metallurgical production method for the metal foam allows for the production of layered structures with cover sheets. The resulting aluminium foam sandwiches (AFS) provide a good thermal interface surface between heat source and storage.

The aim of the present work is to develop a material model based on the material parameters of the foam and the PCM to predict the thermal performance of a paraffin/aluminium foam composite in finite element software. Due to the size of machine tool structures, a discretization fine enough to represent the individual pores of the foam structure is not viable since it would lead to a very large number of degrees of freedom and thereby to very large computation times. Therefore a high resolution numerical study using data from computed tomography is performed and used to derive a reduced representation of the thermal storage compound. In particular the thermal conductivity as a function of the porosity of the foam is of importance since the correlation of these two parameters is not linear [15]. The resulting homogenized material model for the composite is then validated experimentally with paraffin/aluminium foam structures.

## 2. Simulation

### 2.1. Preparation of samples and geometry

Aluminium foam sandwiches (AFS) produced in a powder-metallurgical process according to the procedure described by Seeliger [16] were used for simulation and experiments. The basic material made from aluminium powder (AlMg3Si6) and a foaming agent (TiH<sub>2</sub>) is placed between two sheets made of Al 6082. The foaming is performed at 600 °C for 25 minutes, resulting in an expansion of the middle layer. The procedure leads to a core metallurgically bound to the cover layers. Afterwards the sandwich sheets are planed by rolling and cut into the desired dimensions.

In order to perform a high resolution finite element analysis on a realistic foam structure, a 12 mm wide slice was cut from an AFS-sheet with a total thickness of 12 mm made from 1 mm thick cover layers and 10 mm foamed core, as shown in Fig. 1. The sample was scanned with a GE v|tome|x s 240 micro computed tomograph resulting in images with a resolution of approximately 0.02 mm per pixel over a size of 880 × 897 pixels with the sample being represented by a total of 600 slices. The cover layers were analysed on the basis of the CT-scan. The top cover layer (top side in Fig. 1a) showed the first porosity after 0.61 mm (Fig. 2a and b), the distance between the last porosity and the end of the second cover layer was measured as 0.83 mm. Thus the originally 1 mm thick cover

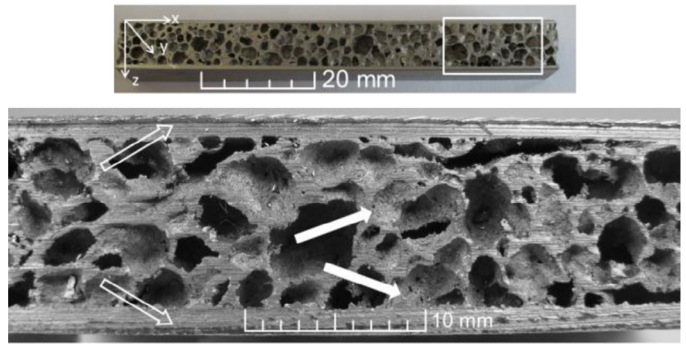


Fig. 1. Top: Slice of AFS used for CT scan, black border indicating scanned volume. Bottom: Detail with cover layers (hollow arrows) and pores including microcracks (filled arrows).

layers were reduced in thickness during the foaming process. Looking at the slice 1 mm below the beginning of the first cover layer (Fig. 2c) a fully developed foam structure is visible, indicating a relevant amount of the cover sheet metal to be partially molten. Therefore a clear separation between the 1 mm thick cover layers and the foam core is not adequate.

The set of CT scan slices was used to create a 3D voxel file. By using the AMDiS meshing tool Meshconv a signed-distance function  $r(x)$  (Fig. 3a) was obtained from the voxel-data, denoting the distance between  $x \in \Omega$ , where  $\Omega$  is the computational domain. The interface  $\Gamma$  is denoted by the zero-level set of  $r(x)$ . The PCM phase is labeled with  $\Omega_{PCM}$ , the aluminium phase with  $\Omega_{Alu}$  and  $r(x)$  is assumed to be negative in  $\Omega_{PCM}$  and positive in  $\Omega_{Alu}$ . From this representation, the porosity of the sample could be evaluated for two partial volumes which are investigated in the following simulations. The first volume has a porosity  $p$  of 70.7%, the second one 62.4%. For the calculation process with a finite element toolbox like AMDiS [17] an implicit representation by phase field values is required (diffuse domain approach) which can easily be constructed from the signed distances as follows [18]:

$$\Phi(x) = \frac{1}{2} \left( 1 - \tanh \left( \frac{3r(x)}{\varepsilon} \right) \right) \quad (1)$$

where  $\varepsilon$  to be 0.005 is proportional to the interface thickness,

$$\Gamma = \left\{ x \mid \Phi \left( x = \frac{1}{2} \right) \right\} \quad \text{and} \quad \Omega_{PCM} \approx 1 \quad \text{and} \quad \Omega_{Alu} \approx 0; \quad \text{see (Fig. 3b).}$$

The volume is meshed with a tetrahedral volume-mesh (Fig. 3c), where at least five grid points are guaranteed in the interface.

### 2.2. Equations

The relaxed linearization scheme by Reference 19 is adopted to solve an enthalpy-based nonlinear heat equation

$$\partial_t H(T) + \nabla \cdot (k \nabla T) = 0, \quad \text{in } \Omega \quad (2)$$

with appropriate initial and boundary conditions. Here  $H$  and  $T$  denote the volumetric enthalpy and temperature, respectively. Through the diffuse domain approach, the thermal conductivity  $k$  of each phase can easily be interpolated to

$$k = k_{PCM} \Phi + (1 - \Phi) k_{Alu} \quad (3)$$

where  $k$  is assumed to be temperature independent. The same way the temperature dependent enthalpy in each phase is calculated from the heat capacities of aluminium and PCM, with

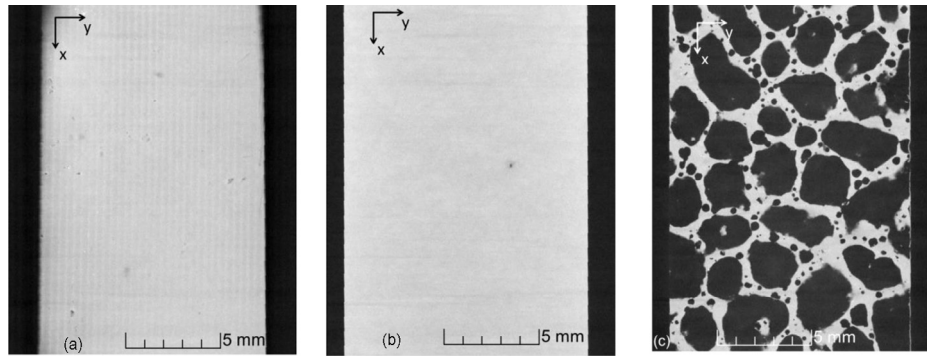


Fig. 2. CT scan images of sample structure. (a) beginning of top cover layer, (b) first pore in cover layer, (c) slice at 1 mm below (a).

$$H_{PCM}(T) = \begin{cases} c_{sPCM} T, & T \leq T_s \\ c_{sPCM} T_s + c_{slPCM} (T - T_s), & T_s \leq T \leq T_l \\ c_{sPCM} T_s + c_{slPCM} (T_l - T_s) + c_{lPCM} (T - T_l), & T \geq T_l \end{cases} \quad (4)$$

and

$$H_{Alu}(T) = c_{sAlu} T \quad (5)$$

we get

$$H(T) = H_{PCM}(T)\Phi + (1 - \Phi)H_{Alu}(T). \quad (6)$$

The temperature range for the phase change is assumed to be non-zero, thereby modelling a mushy phase change in reference to Nedjar [19].

Please note that time independent volumetric heat capacities  $c$  were also adopted. For the description of all variables see Reference 19.

To solve the partial differential equation numerically, the relaxed linearization scheme [19] is implemented in the finite element toolbox AMDiS. In time, a fully implicit discretization is used, where a linearized equation is solved in an iterative procedure until the residual error is less than  $1e-7$ . The time step size is fixed depending on the heat flux, e.g. set to 1 s for heat flux  $1000 \text{ W/m}^2$ . Of course, adaptive time step may also be used.

The computational domain was generated from different clips of CT scan with varying shapes resulting in a size of e.g.  $9.6 \times 13.2 \times 12 \text{ mm}^3$ . To achieve an appropriate spatial discretization, adaptive finite elements were used. Different grid sizes to verify the quality of the computational mesh were performed, and the tests showed that a minimal edge size of  $5.3e-5 \text{ m}$  in the interface of metal and paraffin as well as inside the melting boundary provides good results.

The preconditioned linear system with approximately 6 million unknowns was solved by an iterative CG-solver from the PETSc library [20]. By the use of domain decomposition the domain was split in several parts and each part was solved highly parallel on

up to 512 cores in high performance systems Taurus (ZIH Dresden) and Juropa (Jülich).

### 2.3. Simulation remarks

Two cases were considered, the first one aiming to calculate the effective thermal conductivity parameter  $k_e$  for the material composite. Therefore a heat flux  $q$  was adopted on the top  $\nabla T \cdot n = q$  on  $\delta\Omega_{top}$ , a constant Dirichlet boundary condition  $T = T_D$  on  $\delta\Omega_{bottom}$  and adiabatic boundary conditions on all other remaining boundaries  $\nabla T \cdot n = 0$ . Then  $k_e$  was calculated according to

$$k_e = \frac{q \cdot l}{T_{max} - T_{min}} \quad (7)$$

with  $l$  being the length from top to bottom and  $(T_{max} - T_{min})/l$  the stationary gradient. Please note that  $k_e$  was calculated in temperature regimes where the PCM is solid.

The second case was performed to calculate the transient temperature  $T(t)$  including the melting process of the PCM. Therefore the heat flux on the top was kept and the Dirichlet boundary condition on the bottom was replaced by an adiabatic one.

The material parameters used for the calculations are compiled in Table 1.

Simulations for the first case were evaluated for heat fluxes  $q$  of  $500 \text{ W/m}^2$ ,  $1,000 \text{ W/m}^2$  and  $2,000 \text{ W/m}^2$ ; the second set of simulations was additionally performed with  $50 \text{ kW/m}^2$ ,  $100 \text{ kW/m}^2$ , and  $200 \text{ kW/m}^2$ .

### 2.4. Homogenized model

A reduced model was derived that describes the thermal storage as a homogeneous material, blurring the microstructure of the individual pores. The density for this equivalent material can be calculated based on the porosity  $p$  and the densities of the used materials according to

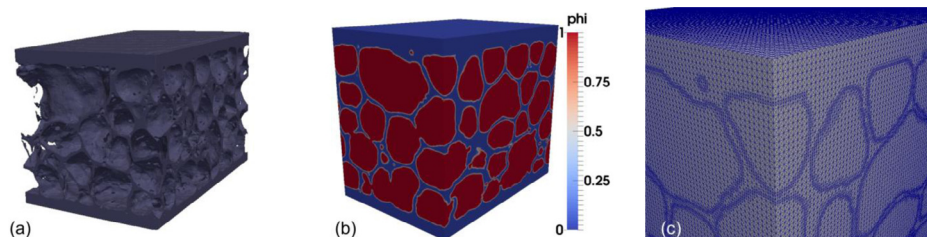


Fig. 3. (a) Interface  $\Gamma$ , zero-level set of  $r(x)$ , (b) phase field  $\Phi(x)$ , (c) tetrahedral volume-mesh.

**Table 1**  
Relevant thermo-physical properties.

Property	Value
<b>Aluminium</b>	
Thermal conductivity $k_{Alu}$	237 W/mK
Specific heat capacity $c_{pAlu}$	897 J/kgK
Density $\rho_{Alu}$	2700 kg/m <sup>3</sup>
<b>PCM (RT 44 HC)</b>	
Thermal conductivity $k_{PCM}$	0.2 W/mK
Specific heat capacity $c_{pPCM}$	2000 J/kgK
Density solid $\rho_{PCM}$	860 kg/m <sup>3</sup>
Density liquid $\rho_{PCM}$	760 kg/m <sup>3</sup>
Start of melting range $T_s$	314 K
End of melting range $T_l$	317 K

$$\rho = (1-p)\rho_{Alu} + p\rho_{PCM} \quad (8)$$

For the temperature dependent enthalpy the partial enthalpies for PCM and aluminium were calculated based on Eqs. (4) and (5) and summed by using

$$H(T) = pH_{PCM}(T) + (1-p)H_{Alu}(T). \quad (9)$$

Several estimates exist for the thermal conductivity of a metal foam structure. It does not scale linearly with the volume fraction [15]. Therefore a more complex model is necessary. A basic upper and lower bound for the estimations can be achieved by modelling the foam structure as a combination of thermal resistances for the solid material and the material contained inside the pores. Assuming a parallel connection of those resistances results in an upper bound and a series connection results in a lower bound for the effective thermal conductivity. Singh and Kasana [21] proposed a model based on a combination of those two bounds according to

$$k_e = k_{||}^F \cdot k_{\perp}^{(1-F)} \quad (10)$$

with  $0 \leq F \leq 1$  where the  $F$ th fraction of the material is oriented in the direction of heat flow and the remaining  $(1-F)$ th fraction is oriented in the perpendicular direction. For description of the parameter  $F$  see Reference 21. The model was verified with experimental data for high porosity structures ( $p > 0.9$ ).

Bhattacharya et al. also proposed a model for open cell foam based on a combination of those two bounds [22]. Boomsma and Poulikakos used a geometry based model for open cell foams [23]. Ashby et al. [14] propose an estimate as valid for both open and closed cell foams stating two bounds based on the density of the foam only according to

$$\left(\frac{\rho_{Foam}}{\rho_{Alu}}\right)^{1.8} < \frac{k_e}{k_{Alu}} < \left(\frac{\rho_{Foam}}{\rho_{Alu}}\right)^{1.65} \quad (11)$$

The four approaches are compared in Fig. 4 for a selected range of porosity. The thermal conductivity of the solid material was assumed to be 237 W/mK, for the liquid phase (paraffin) 0.2 W/mK. The model by Singh was calculated with the parameter  $C$  assumed to be 1, in Batthacharya's model the parameter  $A$  was set to 0.35 and in Boomsma's model the parameter  $e$  was set to 0.339. For detailed discussion of the used parameters, see the respective publications.

Since the results from the high resolution simulation in AMDiS are well fitted by Ashby's lower bound (see Results section), this model is used for the thermal conductivity in the reduced model.

The reduced material model was implemented in the commercial FE-software ANSYS and the second case of the AMDiS-simulations was transferred into a transient thermal model in ANSYS Workbench with the same boundary conditions. The mesh generated used approximately 33,000 nodes, and the problem was solved using a sparse matrix direct solver with automatic time stepping on a single core.

## 2.5. Experimental verification

For further verification of the reduced model, experiments with metal foam sandwich infiltrated with and without PCM were performed.  $200 \times 200$  mm<sup>2</sup> large samples were extracted from an AFS-sheet with a total thickness of 30 mm including 2.5 mm thick cover layers. While the top and bottom side of the matrix was sealed by the metallic bound cover layers, the remaining faces had to be sealed in a second step. At first samples of  $230 \times 230$  mm<sup>2</sup> size were cut out of the AFS-sheet. The top cover layer and the core were then sawed down to  $200 \times 200$  mm<sup>2</sup>, while the bottom aluminium sheet remained. The excess material of the bottom layer was then bent up against the core and the top sheet. The bent over parts were then glued or welded to the top layer to form a completely sealed structure. The leak tightness was checked with compressed air under water and remaining defects were sealed. On two faces, fittings were inserted into holes drilled through the cover sheets into the foam core to act as inlets. These inlets were used for testing the leak tightness as well as for infiltrating the PCM into the foam. The sandwich structure was heated above the melting temperature of the PCM inside an oven and then was placed under suction depression (between  $-0.6$  and  $-0.8$  bar). Then the liquid PCM was filled into the evacuated sandwich using the partial vacuum inside the foam structure. The setup for the infiltration process can be seen in Fig. 5. As phase change material a commercial paraffin with a nominal melting range between 29 and 36 °C was chosen (RT 35 from Rubitherm with the same basic properties as RT 44 HC; see Table 2).

The resulting structure contains PCM in most, but not all pores, as shown in Fig. 6 and also evident from the fill rate in Table 3. This is due to the statistical nature of pore distribution and interconnection.

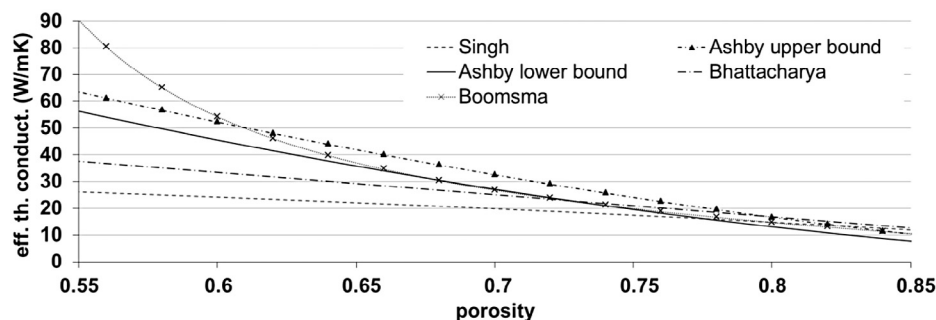


**Fig. 4.** Comparison of theoretical models for thermal conductivity of metal foam.

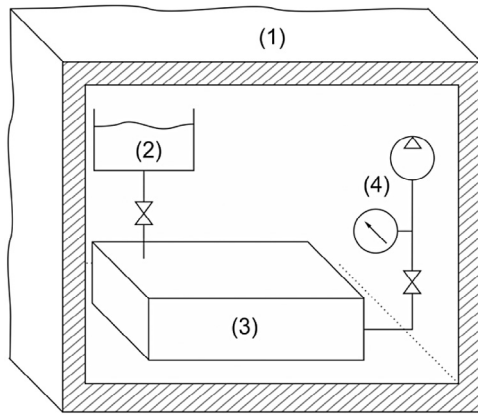


**Fig. 5.** Setup for infiltration procedure: (1) oven, (2) PCM reservoir, (3) sample, (4) vacuum pump and pressure gauge.

Three samples were prepared, two sealed with glue (G1 and G2) and one was welded (W1). The samples were weighed before and after the infiltration-process to determine the density of the foam bodies and the achieved fill rate  $f$  indicating the volume-fraction of pores filled with liquid PCM according to

$$f = \frac{\frac{m_{PCM}}{\rho_{PCM}}}{V_{AFS} - \frac{m_{AFS}}{\rho_{Alu}}} \quad (12)$$

The results are listed in Table 3 with  $c$  denoting the theoretical thermal capacity of the sample below and above the melting range and  $H_{15K}$  the thermal energy needed to heat the sample from 25 to 40 °C. Two more samples were mechanically prepared but not filled with PCM for reference measurements (E1 and E2).

The samples were experimentally investigated in a setup suitable to measure the transient temperature of the structures. Thermocouples of type K were attached to the surface of the samples at three different locations and in the ambient air according to Fig. 7

**Table 2**  
Relevant thermo-physical properties of PCM RT 35.

Property	Value
<b>PCM (RT 35)</b>	
Thermal conductivity $k_{PCM}$	0.2 W/mK
Specific heat capacity $c_{PCM}$	2000 J/kgK
Density solid $\rho_{PCM}$	860 kg/m <sup>3</sup>
Density liquid $\rho_{SPCM}$	770 kg/m <sup>3</sup>
Start of melting range $T_s$	302 K
End of melting range $T_l$	309 K

**Table 3**  
Properties of investigated composite structures.

Sample	Density foam	Mass of PCM	Fill rate	$c$	$H_{15K}$
G1	921 kg/m <sup>3</sup>	0.364 kg	0.577	1769 J/K	76.8 kJ
G2	803 kg/m <sup>3</sup>	0.492 kg	0.696	1936 J/K	96.9 kJ
W1	787 kg/m <sup>3</sup>	0.490 kg	0.722	1870 J/K	95.7 kJ
E1	810 kg/m <sup>3</sup>	–	–	916 J/K	13.7 kJ
E2	797 kg/m <sup>3</sup>	–	–	901 J/K	13.5 kJ

to track the temperature. Measured temperatures were read and recorded with a data logger attached to a computer. The data logger has an accuracy of  $0.2\% \pm 0.5^\circ\text{C}$ . In order to reduce the influence of the ambient air, a layer of insulating material in the form of a fleece made from polyethersulfone fibres with a thermal conductivity of  $0.035 \text{ W/mK}$  was added around the samples. The heat flux was provided by resistive heating foils at the bottom of the sample with an input power of 18.5 W over an area of  $18.400 \text{ mm}^2$ . All samples were heated until the melting temperature of the PCM was clearly exceeded and the temperature rise of the sample was seemingly only due to sensible heating, reaching at least  $40^\circ\text{C}$  at every thermocouple.

The data of the samples were used to calculate the relevant thermal material properties for the reduced model. Taking the partial enthalpy from the PCM datasheet into account, the temperature-dependent enthalpy was calculated for the filled samples. Free convection was used as boundary condition on the outer surfaces of the insulation.

### 3. Results

#### 3.1. Simulations

For different heat fluxes  $q$  the results from AMDiS yielded the same values for the thermal conductivity of the compound structure. Fig. 8 shows the effective thermal conductivity  $k_e$  according to Eq. (7) over time for a domain with 70.7% porosity. The stationary value of  $k_e$  arrived at  $25.4 \text{ W/mK}$  and for a second sample with a porosity of 62.4%  $42.2 \text{ W/mK}$  were reached. The respective values from Ashby's lower bound model are  $26.01 \text{ W/mK}$  and  $40.75 \text{ W/mK}$ . Based on these results, Ashby's prediction was used for the determination of the thermal conductivity of the homogenized material.

The second scenario with heat flux on one side and adiabatic conditions on all other sides resulted in a gradual heating of the compound. In Fig. 9 the temperature profile is shown for several time steps for a high heat flux ( $100 \text{ kW/m}^2$ ). While the aluminium quickly reaches temperatures visibly above the melting range, the pores remain partially solid. The melting interface is indicated in bright colour. This difference in temperatures increases with the applied heat flux and is also visible in the transient temperature-profiles

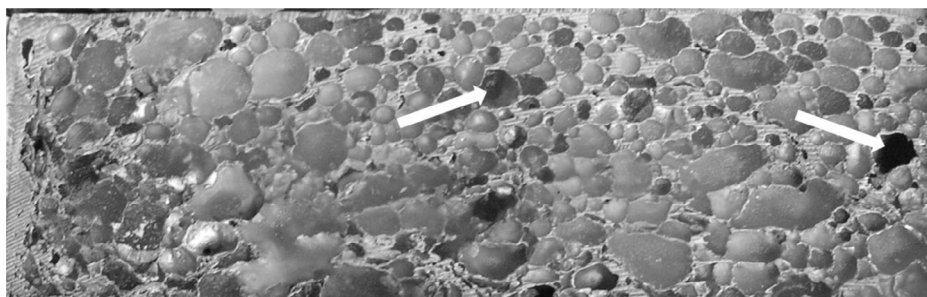


**Fig. 6.** Closed cell metal foam infiltrated with PCM. White arrows indicate not fully filled or completely empty pores.

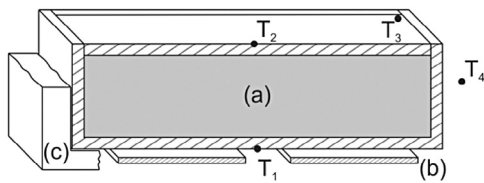


Fig. 7. Setup for thermal testing: (a) sample with foam core and cover layers, (b) resistive heaters, (c) insulation, T1–T4 thermocouples.

shown in Fig. 10 where the difference between minimum and maximum temperature grows with increasing heat flux.

The second set of curves in the transient diagrams shows the results of the homogenized models calculated with ANSYS. Since this model neglects the true geometry of the pores and the moving melting interface inside the PCM phases, a remaining low temperature at the core of the pores vanishes. The impact of this effect also grows with the applied heat flux and thereby results in a larger deviation of the models for high heat fluxes.

### 3.2. Experimental

Fig. 11 shows the temperatures for all five samples until the heating power was turned off. The effect of the phase change is clearly visible due to the delayed temperature rise in the melting range. For comparison between the transient behaviours of all five samples, two main metrics were investigated:  $t_{40}$  is the time it took to heat the sample above  $40\text{ }^{\circ}\text{C}$  and  $dT/dt$  is the rate of temperature rise after the melting range in  $\text{K/s}$ . While the rate of temperature rise indicates the impact of the PCM on the sensible heat capacity

of the compound,  $t_{40}$  shows the combined influence of increased sensible heat capacity and latent heat.

The differences regarding the rate of temperature rise ( $dT/dt$ ) correspond well with the calculated values for the thermal capacity according to Table 4 where the filled samples show a factor of 2 between the filled and the empty samples. In the experiments the rate of temperature rise for the empty samples is twice as high as for the filled samples. Regarding the impact of the latent heat of the PCM the time it takes to heat the sample above its melting temperature is significant: the filled samples take four (G1) to five times (G2) as long as the unfilled structures.

These effects are also reflected in the ANSYS-based simulations with the reduced material model. Fig. 12 shows the results for sample G1 compared to the measured temperatures. The model is fitting the experiments very well with slight deviations after the peak temperature. The differences in the rate of temperature rise before and after the melting process could be explained by the imperfect thermal contact conditions in the experimental setup. Since the heating element is glued to the sample, a contact resistance between the two bodies reduces the heat flux into the sandwich structure, resulting in a slightly lower rate of temperature rise.

### 4. Conclusions

The numerical study regarding the effective thermal conductivity of closed cell metal foam infiltrated with PCM showed that models found in literature, especially the model proposed by Ashby, can be used for the investigated structures. Even though the models are generally only validated for open cell structures with higher porosities, the calculated effective thermal conductivities match the results from a high resolution numerical study.

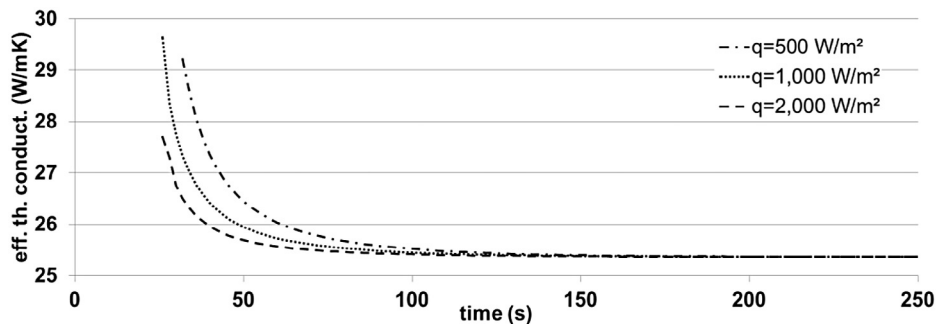


Fig. 8. Thermal conductivity obtained from AMDiS simulations for heat fluxes of 500, 1000 and 2000  $\text{W/m}^2$ .

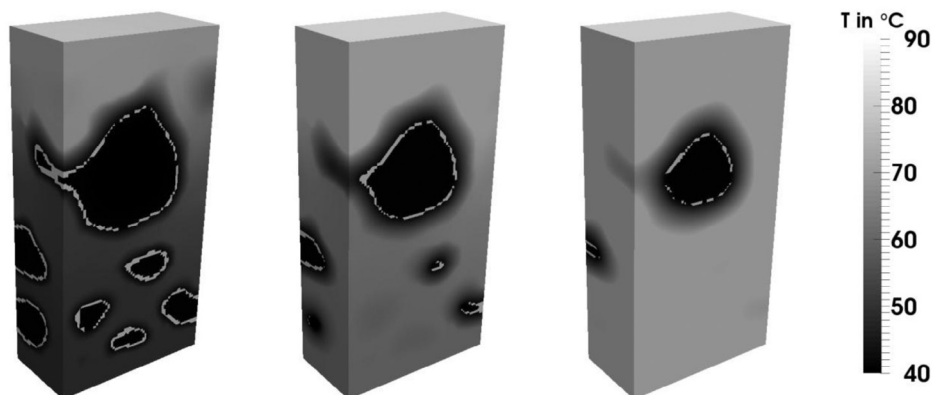


Fig. 9. Temperature profiles from AMDiS simulation with  $100\text{ kW/m}^2$  after 14 s, 19 s and 24 s, starting at  $T = 25\text{ }^{\circ}\text{C}$ .

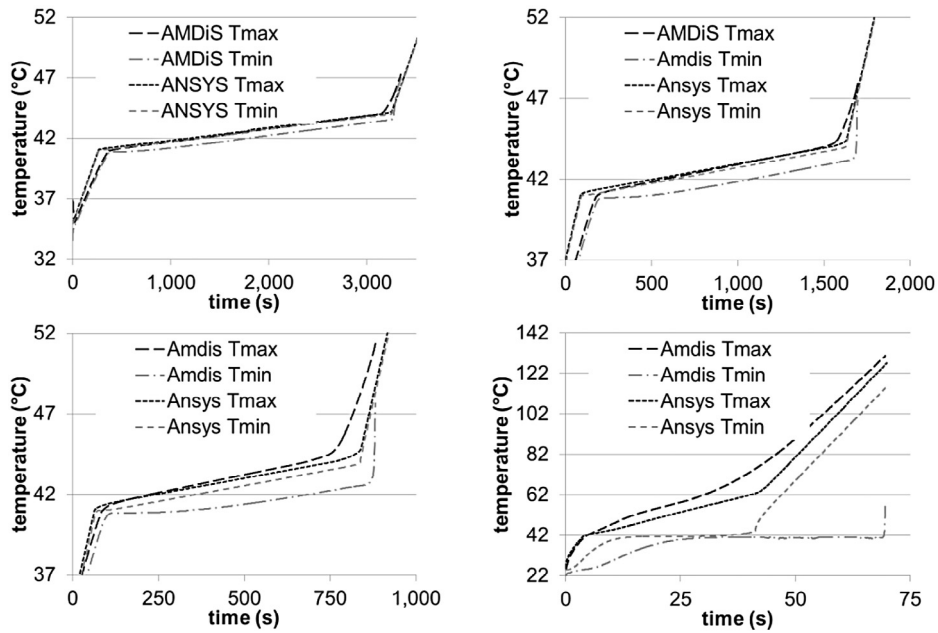


Fig. 10. Time dependent temperature from AMDiS and ANSYS simulations under different heat fluxes (upper left 500 W/m<sup>2</sup>, upper right 1,000 W/m<sup>2</sup>, lower left 2,000 W/m<sup>2</sup>, lower right 50,000 W/m<sup>2</sup>).

A reduced model for a paraffin/metal foam compound neglecting the microstructure of the structure was established. The homogenized material model yields temperature results in good accordance to high resolution numerical simulation as well as experiments. It is suitable for simulation of a thermal storage compound with reduced degrees of freedom for use in large scale models.

The experimental results demonstrate that infiltration with PCM increases the thermal inertia of a metal foam structure in and outside of the PCMs' melting range. Closed cell metal foams are a viable option as matrix material due to their high thermal conductivity. The resulting composite structure is suitable to delay the temperature rise under constant thermal load. In order to use the compound

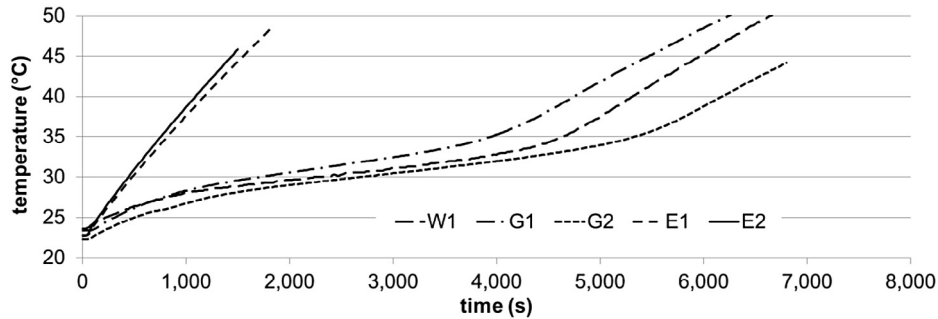


Fig. 11. Transient thermal behaviour of composite structures under constant heat flux.

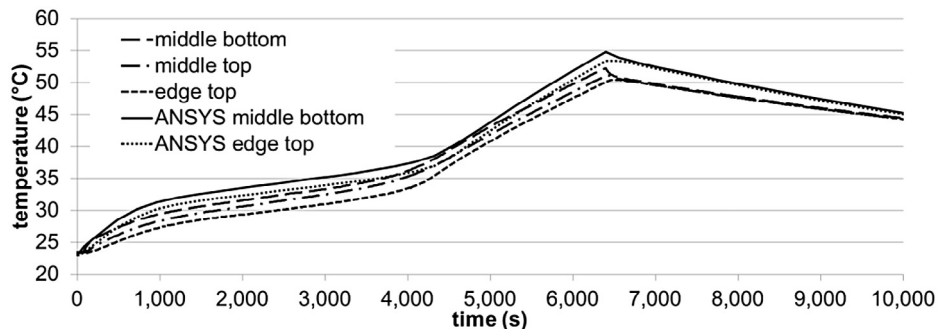


Fig. 12. Experimental and simulation results for sample G1.

**Table 4**

Thermal metrics for investigated samples (time until 40 °C are reached and rate of temperature rise after melting).

Sample	$t_{40}$	$dT/dt$
G1	4750 s	6.3 mK/s
G2	6160 s	7.8 mK/s
W1	5580 s	7.0 mK/s
E1	1175 s	13.4 mK/s
E2	1090 s	14.6 mK/s

to reduce temperature variations under varying thermal load, further experimental and numerical investigations can be conducted.

### Acknowledgements

The authors would like to thank the German Research Foundation (DFG) for financial support within the SFB/Transregio 96 special research centre.

### Nomenclature

A	Parameter for thermal conductivity model by Batthacharya
AFS	Aluminium foam sandwich
C	Parameter for thermal conductivity model by Singh and Kasana
E1, E2	Empty AFS-samples
F	Parameter for thermal conductivity model by Singh and Kasana
FE	Finite element
G1, G2	AFS-samples sealed with glue
H	Volumetric enthalpy (J/m <sup>3</sup> )
$H_{15K}$	Thermal energy needed to heat a sample from 25 to 40 °C (J)
PCM	Phase change material
T	Temperature (°C)
$T_l$	Transition temperature of PCM from mushy to liquid (°C)
$T_s$	Transition temperature of PCM from solid to mushy (°C)
W1	AFS-sample sealed by welding
c	Heat capacity (J/K)
$c_p$	Specific heat capacity (J/kgK)
$dT/dt$	Rate of temperature rise (mK/s)
e	Parameter for thermal conductivity model by Boomsma
k	Thermal conductivity (W/mK)
l	Length of domain (top to bottom of sandwich structure)
p	Porosity (–)
q	Heat flux (W/m <sup>2</sup> )
r	Distance function
t	Time (s)
$t_{40}$	Time to heat a sample from room temperature to 40 °C (s)
x	Location in computational domain

### Greek symbols

$\Gamma$	Interface between phases
$\Phi$	Phase field
$\Omega$	Computational domain
$\partial$	Partial derivative
$\varepsilon$	Interface thickness parameter
$\varrho$	Density (kg/m <sup>3</sup> )
$\nabla$	Nabla operator

### Subscripts

Alu	Aluminium
Foam	Metal foam

PCM	Phase change material
e	Effective
l	Liquid
max	Maximum
min	Minimum
s	Solid
sl	Solid/liquid transition
top	Top side of domain
	Parallel to heat flow
⊥	Perpendicular to heat flow

### References

- [1] J. Bryan, International status of thermal error research, CIRP Ann. Manuf. Technol. 39 (1990) 645–656.
- [2] J. Mayr, J. Jedrzejewski, E. Uhlmann, M. Alkan Donmez, W. Knapp, F. Härtig, et al., Thermal issues in machine tools, CIRP Ann. Manuf. Technol. 61 (2012) 771–791.
- [3] C. Brecher, W. Herfs, C. Heyers, W. Klein, J. Triebs, E. Beck, et al., Resource efficiency of machine tools in the focus of research: enhancing the efficiency of machine tools by optimizing the technologies for operating components. (in german), wt online 100, 559–564, 2010.
- [4] Z. Wang, Z. Zhang, L. Jia, L. Yang, Paraffin and paraffin/aluminum foam composite phase change material heat storage experimental study based on thermal management of Li-ion battery, Appl. Therm. Eng. 78 (2015) 428–436.
- [5] F. Aitlahbib, H. Chehouani, Numerical study of heat transfer inside a Keeping Warm System (KWS) incorporating phase change material, Appl. Therm. Eng. 75 (2015) 73–85.
- [6] A. Mills, M. Farid, J.R. Selman, S. Al-Hallaj, Thermal conductivity enhancement of phase change materials using a graphite matrix, Appl. Therm. Eng. 26 (2006) 1652–1661.
- [7] H. Mehling, L.F. Cabeza, Heat and Cold Storage with PCM: An Up to Date Introduction into Basics and Applications, Springer, Berlin, 2008.
- [8] J.M. Khodadadi, L. Fan, H. Babaei, Thermal conductivity enhancement of nanostructure-based colloidal suspensions utilized as phase change materials for thermal energy storage: a review, Renew. Sustain. Energy Rev. 24 (2013) 418–444.
- [9] L. Fan, J.M. Khodadadi, Thermal conductivity enhancement of phase change materials for thermal energy storage: a review, Renew. Sustain. Energy Rev. 15 (2011) 24–46.
- [10] S.Z. Shuja, B.S. Yilbas, M.M. Shaukat, Melting enhancement of a phase change material with presence of a metallic mesh, Appl. Therm. Eng. 79 (2015) 163–173.
- [11] Y. Li, B. Guo, G. Huang, S. Kubo, P. Shu, Characterization and thermal performance of nitrate mixture/SiC ceramic honeycomb composite phase change materials for thermal energy storage, Appl. Therm. Eng. 81 (25) (2015) 193–197 doi:10.1016/j.applthermaleng.2015.02.008, Available from: <http://www.sciencedirect.com/science/article/pii/S1359431115001167> ISSN 1359-4311.
- [12] J. Chen, D. Yang, J. Jiang, A. Ma, D. Song, Research progress of phase change materials (PCMs) embedded with metal foam (a review), Proc. Mater. Sci. 4 (2014) 369–374.
- [13] K. Lafdi, O. Mesalhy, S. Shaikh, Experimental study on the influence of foam porosity and pore size on the melting of phase change materials, J. Appl. Phys. 102 (2007) 83549.
- [14] M.F. Ashby, C.J. Seymour, D. Cebon, A database of metal foams and honeycombs, in: J. Banhart (Ed.), Metallschäume, Metall Innovation Technologie, MIT, Bremen, 1997, pp. 199–216.
- [15] E. Solórzano, J.A. Reglero, M.A. Rodríguez-Pérez, D. Lehms, M. Wichmann, J.A. de Saja, An experimental study on the thermal conductivity of aluminium foams by using the transient plane source method, Int. J. Heat Mass Transf. 51 (2008) 6259–6267.
- [16] H.-W. Seeliger, Aluminium foam sandwich (AFS) ready for market introduction, Adv. Eng. Mater. 6 (2004) 448–451.
- [17] S. Vey, A. Voigt, AMDiS: adaptive multidimensional simulations, Comput. Vis. Sci. 10 (2007) 57–67.
- [18] X. Li, J. Lowengrub, A. Rätz, A. Voigt, Solving PDEs in complex geometries, Commun. Math. Sci. 7 (2009) 81–107.
- [19] B. Nedjar, An enthalpy-based finite element method for nonlinear heat problems involving phase change, Comput. Struct. 80 (2002) 9–21.
- [20] S. Balay, W.D. Gropp, L.C. McInnes, B.F. Smith, Efficient management of parallelism in object-oriented numerical software libraries 163–202.
- [21] R. Singh, H. Kasana, Computational aspects of effective thermal conductivity of highly porous metal foams, Appl. Therm. Eng. 24 (2004) 1841–1849.
- [22] A. Bhattacharya, V.V. Calmide, R.L. Mahajan, Thermophysical properties of high porosity metal foams, Int. J. Heat Mass Transf. 45 (2002) 1017–1031.
- [23] K. Boomsma, D. Poulidakos, On the effective thermal conductivity of a three-dimensionally structured fluid-saturated metal foam, Int. J. Heat Mass Transf. 44 (2001) 827–836.